  Bull. Chem. Soc. Jpn., 62, 2902—2907 (1989) [Vol. 62, No. 9

A Structural Study of a Series of Bis(2,3-alkanedione dioximato)-nickel(II) Complexes in the Crystal and the Liquid States by X-Ray Absorption Spectroscopy

Seiichi YAMASHITA, Yoshio YANASE, Toshio YAMAGUCHI, and Hisanobu WAKITA*
Department of Chemistry, Faculty of Science, Fukuoka University, Nanakuma, Jonan-ku, Fukuoka 814-01
(Received March 1, 1989)

The structures of a series of bis(2,3-alkanedione dioximato)nickel(II) complexes, [Ni(R,R′-dioxH)$_2$], with dioxH=C(=NOH)-C(=NO), R and R′=H(**A**), R=CH_3 and R′=H(**B**), CH_3(**C**), C_2H_5(**D**), n-C_3H_7(**E**), n-C_4H_9(**F**), n-C_5H_{11}(**G**), n-C_6H_{13}(**H**), or n-$C_{10}H_{21}$(**I**), were investigated in crystals, pyridine solution, and melt (160 °C) by means of extended X-ray absorption fine structure (EXAFS) and X-ray absorption near edge structure (XANES), magnetic susceptibility, and UV/visible spectra. The magnetic susceptibility of complexes **C**, **F**, and **H** in crystals revealed a diamagnetic character. The electronic spectra of crystalline samples **E**, **F**, and **H** changed with the alkyl substituents of the glyoximato ligands, while the corresponding spectra in a pyridine solution were very similar to each other, independent of the glyoximato ligands. The EXAFS data showed that the average Ni–N distance within nickel(II) glyoximato complexes is 1.85—1.88 Å, practically independent of the alkyl substituents of the glyoximato ligands. The XANES spectra were found to correlate with the molecular packing structures of nickel(II) glyoximato complexes in crystals, pyridine solutions, and melt.

A series of 2,3-alkanedione dioximes are known as a good precipitant for Ni(II) and Pd(II) ions. The crystal structures of bis(2,3-alkanedione dioximato) nickel(II) complexes (Fig. 1) were reported for bis(dioximato)nickel(II), [Ni(gH)$_2$],[1] bis(2,3-butanedione dioximato)nickel(II), [Ni(dmgH)$_2$],[2] and bis(2,3-pentanedione dioximato)nickel(II), [Ni(emgH)$_2$].[3] In the crystal structure of [Ni(dmgH)$_2$], planar Ni(II) complexes are stacked face to face along the c-axis to form Ni···Ni linear chains;[4] hereafter, this molecular packing structure is referred to as the cross-type[5] ((b) and (d) in Fig. 2). On the other hand, for the crystal structures of [Ni(gH)$_2$] and [Ni(emgH)$_2$], planar Ni(II) complexes are arrayed like the slats of a venetian blind; this molecular packing structure is referred to as the blind-type[5] ((a) and (c) in Fig. 2). The molecular packing structure of the blind-type for [Ni(emgH)$_2$] complex is transformed into the cross-type by heating.[5] On the other hand, bis(2,3-alkanedione dioximato)-nickel(II) complexes in pyridine, acetone, and alcohols solutions show the same red-orange color as that in the crystalline state,[6] suggesting that no solvent molecule coordinates to a central nickel(II) ion. Moreover, [Ni(R,R′-dioxH)$_2$] complexes with long alkyl chains R′ (**E**—**I**) can be melted and sublimed by heating.

In spite of the above interesting phenomena, there are no comprehensive structural analyses of a series of bis(2,3-alkanedione dioximato)nickel(II) complexes in crystals, solution, and melt. In the present paper, the structures of the [Ni(R,R′-dioxH)$_2$] complexes given in Table 1 have been investigated in solid, pyridine solution, and melt by EXAFS[7] and XANES[8] spectra, magnetic susceptibility,[9] and UV/visible spectral measurements, in particular, to examine the effect of the length of the alkyl chains in glyoximato ligands on the molecular structure of the Ni(II) complexes and to reveal structural differences between the Ni(II) complexes in the three states.

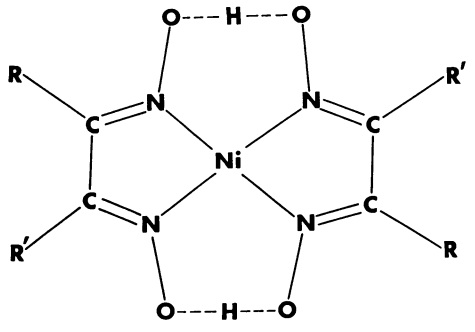

Fig. 1. Molecular structure of [Ni(R,R′-dioxH)$_2$].

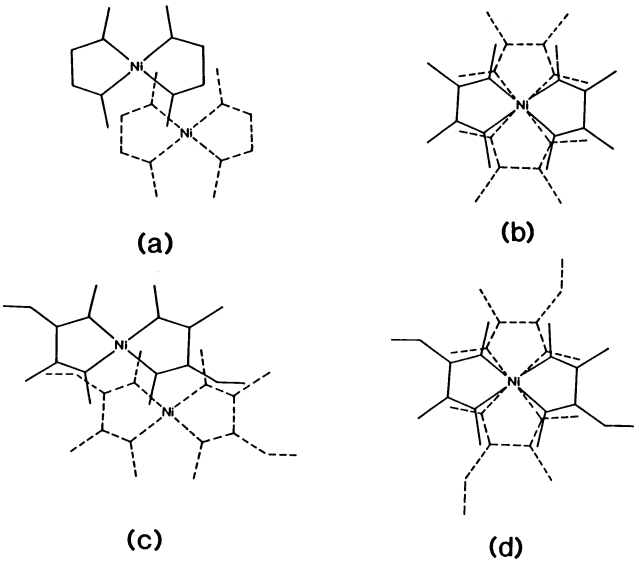

Fig. 2. Molecular packing structures for crystals of [Ni(R,R′-dioxH)$_2$]. (a) The blind-type for [Ni(gH)$_2$],[1] (b) the cross-type for [Ni(dmgH)$_2$],[2] (c) the blind-type for [Ni(emgH)$_2$],[3] and (d) the cross-type for thermally transformed [Ni(emgH)$_2$].[3]

Experimental

Sample Preparation. A series of 2,3-alkanedione dioximes were prepared as reported in the literature[5] and recrystallized from a mixture of methanol and chloroform.

Bis(2,3-alkanedione dioximato)nickel(II) complexes (Table 1) were prepared in the following manner. An aqueous solution, saturated with $[Ni(CH_3COO)_2]4H_2O$, was added to a hot concentrated methanol solution of a dioxime ligand. The complex formed was recrystallized more than five times from a mixture of methanol and chloroform, and then dried in a vacuum desiccator. They were identified by ^{13}C NMR spectrometry, X-ray powder diffractometry and thermal analysis.

Magnetic Susceptibility Measurements. For crystalline powder of complexes **C**, **F**, and **H**, and a pyridine solution and melt of complex **F**, the magnetic susceptibility was measured by a hand-made thermomagnetic analysis (TMA) system equipped with a temperature control unit.[9] The voltage, the electric current, and the intensity of the magnetic field used in the measurements were 50 V, 7A, and 1.6 T, respectively. A reference compound used for calibration of TMA was powdery $[Ni(en)_3]S_2O_3$, which had been purified by recrystallization from water twice.

UV/Visible Spectral Measurements. UV/visible spectra were measured over the wavelength from 400 to 600 nm with a Hitachi spectrophotometer U-3200. The opal method was used for crystalline samples, while the liquid film method was employed for pyridine solutions.

X-Ray Absorption Measurements. X-Ray absorption measurements were performed at the BL-10B station of the Synchrotron Radiation Research Facility (the Photon Factory) in the National Laboratory for High Energy Physics (KEK). X-Ray absorption data were collected in the range from ca. 400 eV on the lower energy side of the nickel *K*-edge (8331.7 eV) to ca. 1800 eV on the higher energy side.

Table 1. Composition of $[Ni(R,R'\text{-dioxH})_2]$

	Complex	R	R′
A	$[Ni(gH)_2]$	H	H
B	$[Ni(mgH)_2]$	CH_3	H
C	$[Ni(dmgH)_2]$	CH_3	CH_3
D	$[Ni(emgH)_2]$	CH_3	C_2H_5
E	$[Ni(mprgH)_2]$	CH_3	n-C_3H_7
F	$[Ni(bmgH)_2]$	CH_3	n-C_4H_9
G	$[Ni(mpegH)_2]$	CH_3	n-C_5H_{11}
H	$[Ni(hxmgH)_2]$	CH_3	n-C_6H_{13}
I	$[Ni(decmgH)_2]$	CH_3	n-$C_{10}H_{21}$

The time to collect X-ray photons was 2 seconds at each measuring point. Crystalline samples were measured in a pellet form after powdering crystals with an agate mortar. Pyridine solution samples, prepared by dissolving crystalline Ni(II) complexes in distilled pyridine, were measured with a polyethylene pouch sandwiched by polyacrylate holders. Melting samples were measured at 160 °C by use of a metallic cell on a hot-plate.

EXAFS spectra were analysed as previously reported.[7] The structural parameters (the interatomic distance, the mean-square displacement, and the coordination number) were determined by a curve fitting method applied to Fourier filtered EXAFS spectra. The basic formula are described below.

The observed EXAFS spectrum, $\chi_{obsd}(k)$, is Fourier transformed to a function, $F(r)$, by the following equation.

$$F(r) = \int_{k_{min}}^{k_{max}} k^3 \cdot \chi_{obsd}(k) \cdot \exp(2ikr)dk \quad (1)$$

$$= F_{re}(r) + iF_{im}(r), \quad (2)$$

where k is the photoelectron wavenumber, $F_{re}(r)$ and $F_{im}(r)$ are the real and imaginary parts of the $F(r)$ function, respectively. k_{max} and k_{min} are the upper and lower k-values used in the transform. The radial function, $|F(r)|$, is given as

$$|F(r)| = [F_{re}(r)^2 + F_{im}(r)^2]^{1/2}. \quad (3)$$

The calculated EXAFS spectrum, $\chi_{calcd}(k)$, is given as

$$\chi_{calcd}(k) = \sum_j [N_j/(k \cdot r_j^2)] \cdot |f_j(\pi, k)| \cdot \sin(2kr_j + \phi_j(k)) \cdot \exp(-2r_j/\lambda_j) \cdot \exp(-2\sigma_j^2 k^2), \quad (4)$$

where r_j is the distance from an absorbing to backscattering atoms in the j-th coordination shell, N_j the number of the backscattering atoms at r_j, σ_j^2 the mean square displacement, and λ_j the mean free path. $|f_j(\pi,k)|$ and $\phi_j(k)$ are, respectively, the backscattering amplitude and the phase shift of the atoms in the j-th shell. A curve fitting is performed to minimize an error-square sum, U, as

$$U = \sum[k^3 \cdot \chi_{filt}(k) - k^3 \cdot \chi_{calcd}(k)]^2, \quad (5)$$

where $\chi_{filt}(k)$ is the Fourier backfiltered EXAFS spectrum.

Results

Magnetic Susceptibilities. The measured magnetic susceptibility of complexes **C**, **F**, and **H** is listed in Table 2. In the case of crystalline samples **C**, **F**, and **H**,

Table 2. Magnetic Susceptibility Measured for Complexes **C**, **F**, and **H**. χ_{Ni}, μ_B, and T Are the Magnetic Susceptibility Per Mole of Ni Atom, Bohr Magneton, and Temperature Measured, Respectively

	Sample		$\chi_{Ni}/10^{-6}$ cm^3 mol^{-1}	μ_B/BM	T/°C
C	$[Ni(dmgH)_2]$	Crystal	−34.0		20
F	$[Ni(bmgH)_2]$	Crystal	−27.0		20
		Melt	4.45	0.12	160
		Solution[a]	125	0.54	20
H	$[Ni(hxmgH)_2]$	Crystal	−22.6		20

a) Pyridine solution.

the magnetic susceptibility per mole of Ni, χ_{Ni}, measured at 20 °C was all negative. On the other hand, the χ_{Ni} values of a melt of sample **F** at 160 °C and of a pyridine solution of sample **F** at 20 °C became both slightly positive.

UV/Visible Spectra. Figure 3 shows the electronic spectra for complexes **E**, **F**, and **H** in crystals and pyridine solutions. The spectra of the crystalline samples (solid lines in the figure) show different d–d transition bands in the wavelength range from 430 to 550 nm, depending on the complexes. For the corresponding pyridine solutions, however, all spectra (dashed lines) resemble each other with a shoulder at about 480 nm.

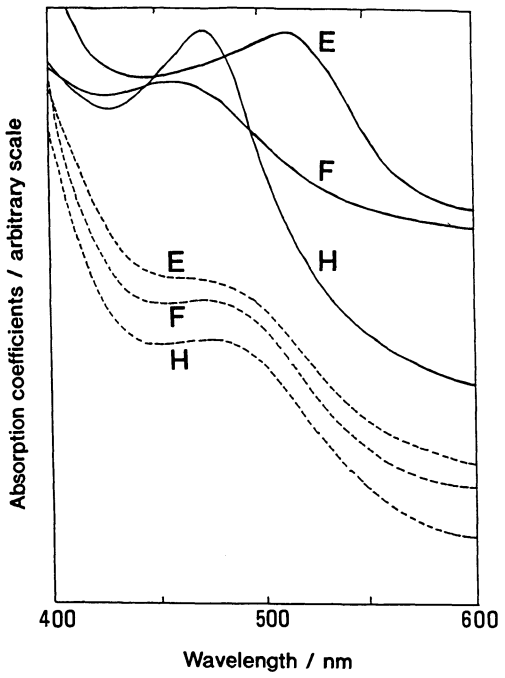

Fig. 3. UV/visible spectra of complexes **E**, **F**, and **H**. Solid lines; crystal, dashed lines; pyridine solution.

EXAFS Analysis. Figures 4 and 5 show the experimentally obtained $k^3\chi(k)$ curves of the crystalline powder of complexes **A**—**I**, and of pyridine solutions and melts of complexes **E**, **F**, and **H** respectively. The corresponding radial function curves (uncorrected for the phase shift) are shown in Figs. 6 and 7; the k range used in the Fourier transform was from 4.5 to 14.0 Å^{-1} for all the spectra. The prominent first peak at about 1.5 Å in each radial function is ascribable to Ni–N interactions within [Ni(R,R′-dioxH)$_2$] complexes. The second and third peaks observed at 2.5—4.0 Å should be ascribed to nonbonded Ni···C and Ni···O interactions within the complexes. The peaks appearing beside the sharp Ni–N peak are the side lobe.

In order to obtain the structural parameters of the Ni–N interactions, Fourier filtered EXAFS spectra were extracted for the first peak from 1.1 to 1.9 Å in the radial functions. Subsequently, the theoretical function of Eq. 4 was fitted to the filtered spectra from 5.5 to 13.0 Å^{-1} in the k space. The backscattering amplitude and phase shift for the Ni–N interaction were determined by a least-squares method for reference compound of known structure **A**. In the fits

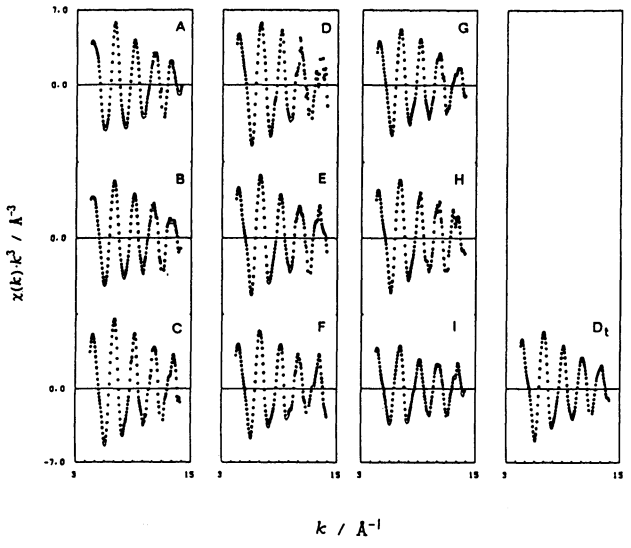

Fig. 4. Observed EXAFS, $k^3\chi(k)$, spectra for crystalline samples **A**—**I** and $\mathbf{D}_t$. $\mathbf{D}_t$ is thermally transformed crystal **D**.

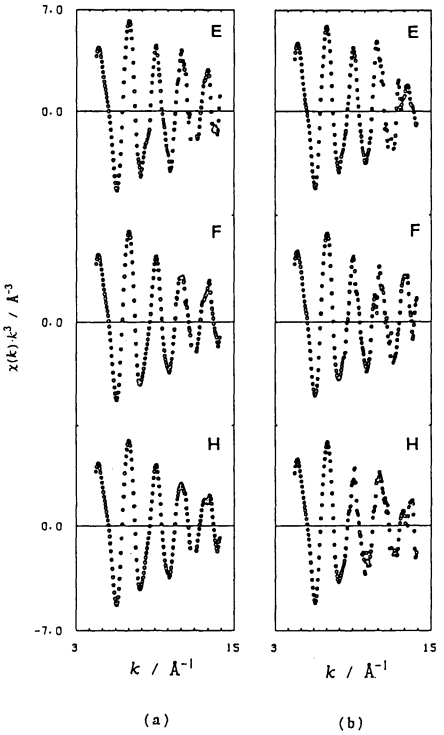

Fig. 5. Observed EXAFS, $k^3\chi(k)$, spectra for solutions and melts of complexes **E**, **F**, and **H**. (a) Pyridine solutions (b) melts (160 °C).

Table 3. Ni–N Interatomic Distances in Crystal, Pyridine Solution, and Melt Obtained from the EXAFS Analysis on the Basis of the One-Shell Model for the Ni–N Interactions. The Values in Parentheses Are X-Ray Diffraction Data

	Complex	r/Å		
		Crystal	Solution[a]	Melt[b]
A	$[Ni(gH)_2]$[c]	1.88 (1.87,[d] 1.88[d])		
B	$[Ni(mgH)_2]$	1.88		
C	$[Ni(dmgH)_2]$	1.87 (1.87,[e] 1.90[e])		
D	$[Ni(emgH)_2]$	1.85 (1.83,[f] 1.88[f])		
$\mathbf{D_t}$	$[Ni(emgH)_2]$[g]	1.88		
E	$[Ni(mprgH)_2]$	1.88	1.88	1.88
F	$[Ni(bmgH)_2]$	1.88	1.87	1.88
G	$[Ni(mpegH)_2]$	1.88		
H	$[Ni(hxmgH)_2]$	1.88	1.86	1.88
I	$[Ni(decmgH)_2]$	1.86		

a) Pyridine solution. b) Measured at 160 °C. c) Structure standard. d) Ref. 1. e) Ref. 2 (poor R-value=0.16). f) Ref. 3. g) Thermally transformed crystal **D**.

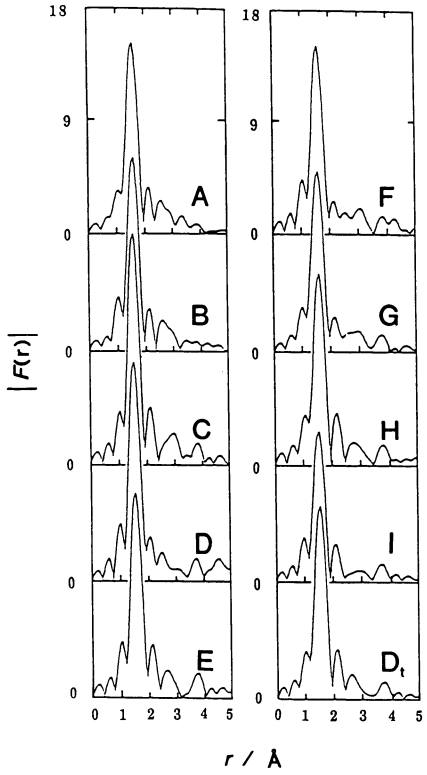

Fig. 6. The radial functions, $|F(r)|$, for crystalline samples **A**—**I** and $\mathbf{D_t}$. $\mathbf{D_t}$ is thermally transformed crystal **D**.

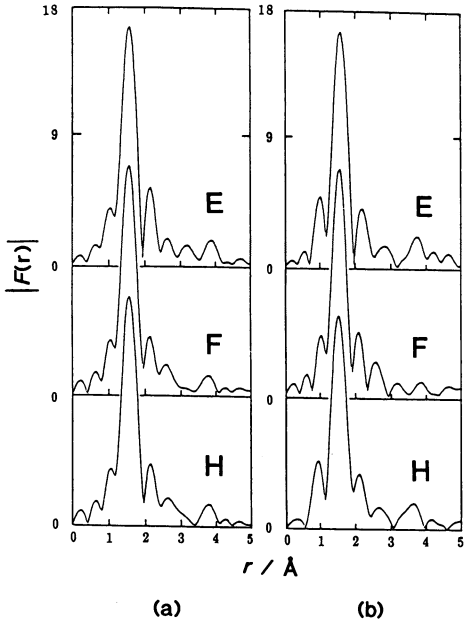

Fig. 7. The radial functions, $|F(r)|$, for solutions and melts of complexes **E**, **F**, and **H**. (a) Pyridine solutions (b) melts (160 °C).

different Ni–N interactions in the crystal (1.87 and 1.88 Å) were treated as one-shell since the difference in the Ni–N distances was within the uncertainties in the EXAFS analysis; the average bond distance and the coordination number were fixed at 1.88 Å and 4,[1] respectively.

Table 3 summarizes the Ni–N interatomic distance within the complexes in crystals, pyridine solutions, and melts obtained from the curve-fittings. The Ni–N bond lengths fall within 1.85 — 1.88 Å independent of the alkyl substituents and the sample states.

In the curve fits of the Ni–N interactions for complexes **E**, **F**, and **H** in pyridine solutions the coordination numbers of four and six were tested for Ni(II)-coordination; the best fit was obtained only when the coordination number was four. This result shows that no pyridine molecules coordinate to a central nickel(II) ion. Therefore, in subsequent curve fits of pyridine solutions of complexes **E**, **F**, and **H** the coordination number was kept constant at four.

XANES Patterns. Figures 8 and 9 show, respectively, the XANES curves for crystals of complexes **A**—**I** and for pyridine solutions and melts of complexes **E**, **F**, and **H**. The XANES curves in the X-ray energy range from 8310 to 8380 eV can be classified into three kinds of patterns, which are referred subsequently to as α-, β-, and γ-patterns. In the three kinds of XANES

patterns were observed a pre-edge peak at 8330 eV and two peaks at 8348 — 8362 eV. The α-, β-, and γ-patterns correspond, respectively, to that of crystalline samples **A**, **B**, and **D**, that of crystalline samples **C**, **E**—**I**, and $\mathbf{D}_t$, and that of solution samples **E**, **F**, and **H**.

The α-pattern was characteristic of a shoulder at 8336 eV, while the β-pattern had a sharp peak at 8335 eV and a shoulder at 8342 eV. On the other hand, the γ-pattern observed for the pyridine solutions showed no distinct peak at 8335 — 8345 eV, but appreciable shoulders at 8337 and 8342 eV. The XANES curves of the melts of complexes **E**, **F**, and **H** showed the β-pattern.

Discussion

Crystalline State. As seen in Table 3, the Ni–N interatomic distances for crystalline samples **B** — **I** do not change significantly with the length of the alkyl substituents in the glyoximato ligands. In addition, the magnetic susceptibility (Table 2) of crystalline samples **C**, **F**, and **H** is all negative; thus, these [Ni(R,R′-dioxH)$_2$] complexes are diamagnetic in crystals. These experimental results indicate that the square planar NiN_4 skeleton within a series of the [Ni(R,R′-dioxH)$_2$] complexes is not significantly distorted in the solid state.

However, the XANES patterns (Fig. 8) of the crystalline [Ni(R,R′-dioxH)$_2$] complexes have shown different features (the α- and β-types) as mentioned in the previous section. The pre-edge peak due to the 1s→3d electron transition of nickel(II) ion observed at 8330 eV in all spectra does not show any remarkable change with respect to the shape and peak position. This fact indicates that the oxidation state of nickel atom in crystalline samples **B**—**I** is very similar to

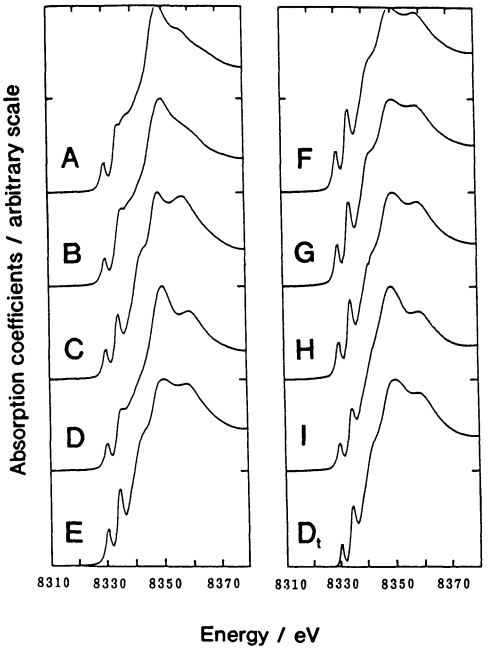

Fig. 8. The XANES spectra of crystalline samples **A**—**I** and $\mathbf{D}_t$. $\mathbf{D}_t$ is thermally transformed crystal **D**.

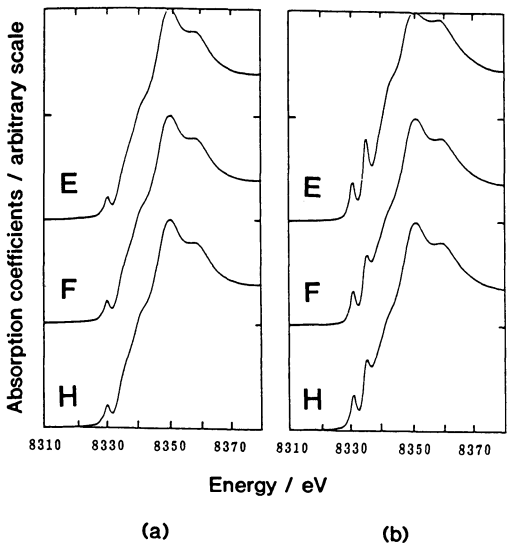

Fig. 9. The XANES spectra of solutions and melts of complexes **E**, **F**, and **H**. (a) Pyridine solutions, (b) melts (160 °C).

Table 4. Packing Structures and XANES Patterns (Figs. 8 and 9) Found for [Ni(R,R′-dioxH)$_2$] Complexes in Crystals, Melts, and Pyridine Solutions. The α, β, and γ Refer to the Packing Types Described in the Text

	Complex	Crystal		Solution[a]	Melt[b]
		Packing	XANES	XANES	XANES
A	[Ni(gH)$_2$]	Blind	α		
B	[Ni(mgH)$_2$]		α		
C	[Ni(dmgH)$_2$]	Cross	β		
D	[Ni(emgH)$_2$]	Blind	α		
$\mathbf{D}_t$	[Ni(emgH)$_2$][c]	Cross	β		
E	[Ni(mprgH)$_2$]		β	γ	β
F	[Ni(bmgH)$_2$]		β	γ	β
G	[Ni(mpegH)$_2$]		β		
H	[Ni(hxmgH)$_2$]		β	γ	β
I	[Ni(decmgH)$_2$]		β		

a) Pyridine solution. b) Measured at 160 °C. c) Thermally transformed crystal **D**.

each other, independent of the length of the alkyl chains in glyoximato ligands. Therefore, the variation of the XANES curves may be due to the change in the electronic state of nickel(II) ion influenced by neighboring atoms: the change in the symmetry around Ni(II) ion and/or different multiple scattering processes arising from different surroundings of Ni(II) ion in the complexes, i.e. different crystal packings.

Table 4 compares the crystal packing structures of Ni(II) glyoximato complexes with their XANES patterns. According to the crystal structures reported,[1-3] the packing form of complexes **A** and **D** is of the blind-type ((a) and (c) in Fig. 2); the corresponding XANES curves show the α-pattern. On the other hand, complexes **C** and $\mathbf{D_t}$ have the cross-type packing structure ((b) and (d) in Fig. 2); their XANES curves belong to the β-pattern. The crystal structures of complexes **B** and **E—I** are not available in the literature. X-Ray diffraction patterns were measured for all the powdered samples **A—I**, but none of these was found to be isomorphic; thus the packing structures of complexes **B** and **E—I** could not be estimated from the X-ray powder patterns. It is suggested, however, from UV/visible spectral measurements[5] that the crystal packing of complex **E** is similar to that of complex **C** with the cross-type packing structure.

In spite of the above limited number of the crystal structures reported for [Ni(R,R'-dioxH)$_2$] complexes, we may discuss the correlation between the XANES patterns and the packing types in the crystal structure. As seen in Fig. 2, in the case of the packing structure of the blind-type, the axial sites above and below a central Ni atom are occupied by light (oxygen, nitrogen, and carbon) atoms, while for the packing structure of the cross-type nickel atoms in other layers are above and below a central Ni(II) ion. Thus, the different feature in the XANES spectra shown in Figs. 8 and 9 is probably ascribed to the different types of the interactions between an Ni(II) ion and the atoms present above and below the Ni(II) ion since the electronic state of Ni(II) glyoximato complexes or the multiple scattering process through different backscattering atoms will change. This conclusion is also supported from the experimental finding that the γ-pattern is observed for all pyridine solutions (Fig. 9), in which no pyridine molecule directly coordinates to a central nickel(II) ion.

On the basis of the above relation between the XANES patterns and the packing types we may presume a packing structure of the other complexes whose crystal structures are not known. Since the XANES curve of complex **B** shows the α-pattern, the complex probably has the blind-type packing structure. Similarly, from the XANES curves of complexes **E—I** showing the β-pattern, the packing structure of the complexes may be of the cross-type.

Solutions and Melts. Unlike the crystalline compounds, the solution and melt of sample **F** showed a slightly positive value (0.54 and 0.12 BM) of their magnetic susceptibility (Table 2). The positive magnetic susceptibility of bis(2-propanedione dioximato)nickel(II) in pyridine solution was reported to be 1.5 BM.[10]

In pyridine solutions the electronic spectra of the three complexes (**E**, **F**, and **H**) resemble each other (Fig. 3), independent of the length of the alkyl substituents, so do the XANES spectra (Fig. 9). From these experimental findings the complexes **E**, **F**, and **H** may have a similar NiN_4 moiety in pyridine solutions.

For melts of complexes **E**, **F**, and **H**, the Ni–N interatomic distances and the XANES patterns are similar to those in crystals (Table 3). The XANES spectra of the melts show the β-pattern, suggesting that the complex molecules in the melts still retain cross-type packing structure, similar to that found in the corresponding crystals.

The authors wish to thank Dr. Masaharu Nomura for his advice in the X-ray absorption spectral measurements and Dr. Mikiya I for his help in preparation of the compounds. This work has been performed under the approval of the Photon Factory Program Advisory Committee (Proposal No. 86-008). All the calculations were performed with an FACOM M-380 R computer at the Computer Center of Fukuoka University.

References

1) M. Calleri and G. Ferraris, *Acta Crystallogr.*, **22**, 468 (1967).

2) L. E. Godycki and R. E. Rundle, *Acta Crystallogr.*, **6**, 487 (1953).

3) R. H. Bowers, C. V. Banks, and R. A. Jacobson, *Acta Crystallogr., Sect. B*, **28**, 2318 (1972); A. G. Sharpe and D. B. Wakefield, *J. Chem. Soc.*, **1957**, 281; B. Egneus, *Anal. Chim. Acta*, **48**, 291 (1969).

4) S. Yamada and R. Tsuchida, *Bull. Chem. Soc. Jpn.*, **27**, 156 (1954); C. V. Banks and D. W. Barnum, *J. Am. Chem. Soc.*, **80**, 3579 (1958); J. C. Zahner and H. G. Drickamer, *J. Chem. Phys.*, **33**, 1625 (1960); C. V. Banks and S. Anderson, *Inorg. Chem.*, **2**, 112 (1963).

5) M. I, H. Wakita, and I. Masuda, *Bull. Chem. Soc. Jpn.*, **56**, 1627 (1983).

6) S. Shinra, *Kagaku*, **19**, 939 (1963).

7) Y. Tajiri and H. Wakita, *Bull. Chem. Soc. Jpn.*, **59**, 2285 (1986); Y. Tajiri and H. Wakita, *Nippon Kagaku Kaishi*, **11**, 1531 (1986); "EXAFS Spectroscopy," ed by B. K. Teo and D. C. Joy, Plenum Press, New York (1981).

8) "EXAFS and Near Edge Structure," ed by A. Bianconi, L. Incoccia, and S. Stipcich, Springer Series in Chemical Physics 27 of International Conference, Tokyo (1982).

9) K. Miyokawa and I. Masuda, *Fukuoka Univ. Sci. Rep.*, **10**, 85 (1980).

10) J. B. Willis and D. P. Mellor, *J. Am. Chem. Soc.*, **69**, 1237 (1947).